

**Optimization of pendant chain length in partially fluorinated aromatic anion exchange membranes for alkaline fuel cells**

Journal:	<i>Journal of Materials Chemistry A</i>
Manuscript ID	TA-ART-05-2018-004310.R1
Article Type:	Paper
Date Submitted by the Author:	18-Jun-2018
Complete List of Authors:	Mohamed Ahmed Mahmoud, Ahmed; University of Yamanashi, Clean Energy Research Center Miyatake, Kenji; University of Yamanashi, Clean Energy Research Center



Journal Name

ARTICLE

## Optimization of pendant chain length in partially fluorinated aromatic anion exchange membranes for alkaline fuel cells

Ahmed Mohamed Ahmed Mahmoud<sup>ab</sup> and Kenji Miyatake<sup>\*a</sup>Received 00th January 20xx,  
Accepted 00th January 20xx

DOI: 10.1039/x0xx00000x

[www.rsc.org/](http://www.rsc.org/)

For robust anion exchange membranes, we have investigated the effect of aliphatic side chains on the properties of partially fluorinated aromatic copolymers (QPAF) with ammonium groups. A new series of QPAF membranes with various interstitial aliphatic side chain lengths (QPAF-Cx) where x = 2-6 were successfully synthesized. QPAF-C3 with propylene side chain and ion exchange capacity (IEC = 1.24 meq. g<sup>-1</sup>) showed balanced properties with the highest hydroxide ion conductivity (99 mS cm<sup>-1</sup> at 80 °C in water) with relatively low water uptake, based on well-developed phase separated morphology. Moreover, QPAF-C3 membrane exhibited excellent alkaline stability to maintain high ion conductivity (98% remaining) and high mechanical properties after 1000 h in 1 M KOH at 80 °C. QPAF-C3 membrane also revealed reasonable stability even in 4 M and 8 M KOH at 80 °C. In fuel cell operation, QPAF-C3 membrane exhibited higher power density (224 mW cm<sup>-2</sup>) than those of our previous QPAF-C1 (138 mW cm<sup>-2</sup>), QPAF-C1B (167 mW cm<sup>-2</sup>), and Tokuyama A 201 (122 mW cm<sup>-2</sup>) membranes. In durability test for 62 h, QPAF-C3 maintained 69% of its initial voltage with minor structural degradation.

### 1. Introduction

Anion exchange membranes have attracted tremendous attention in the last decade due to their potential applications in redox flow batteries, electro dialysis, water electrolysis (hydrogen production), water purification, and anion exchange membrane fuel cells (AEMFCs).<sup>1-4</sup> In particular, a significant number of research on AEMFCs has been documented due to their cost effectiveness compared to proton exchange membrane fuel cells (PEMFCs) thanks to alkaline environments that enable the use of less expensive non-platinum group metals as electrocatalysis.<sup>6</sup> However, the existing AEMs underperform the PEMs in terms of the ion conductivity and chemical stability.<sup>5</sup> The mobility of hydroxide ion is lower than that of proton to cause lower conductivity of AEMs compared to PEMs.<sup>7</sup> Most AEMs carry quaternary ammonium groups as counter ions to anions, which suffer from chemical degradation *via* several different mechanisms under alkaline conditions.<sup>8-11</sup> Therefore, improvement of the trade-off relationship between the ion conductivity and chemical stability has been the most critical issue for AEMs.

Through a number of research works, it has been recognized that trimethylbenzyl ammonium groups are prone to the nucleophilic attack by the hydroxide ions. To mitigate

the nucleophilic decomposition, replacing one or two methyl groups on the benzyl ammonium groups with other substituents such as longer alkyl and/or bulky (hetero)cyclic groups has been investigated.<sup>12-15</sup> Alternative cationic groups including phosphonium, guanidinium, and transition metal ions have been explored.<sup>16-18</sup> Composite membranes have also been investigated recently.<sup>19,20</sup> Some of these AEMs were claimed to exhibit better chemical stability under harsh alkaline conditions than those with typical trimethyl benzyl ammonium groups,<sup>12,14</sup> however, their trade-off relationship needs further improvement for practical applications. Recently, several research groups have reported that introducing interstitial aliphatic groups between the polymer main chain (mostly phenylene groups) and the ammonium groups was effective to suppress the SN2 degradation and Hofmann elimination (experienced to  $\beta$ -hydrogen atoms attached to the ammonium groups via E2 mechanism).<sup>15,21-26</sup> The optimum length of the interstitial aliphatic groups seemed to differ among the different polymer main chains since the effect of the side chains on hydroxide ion conductivity was not identical. Therefore, the interstitial aliphatic groups have to be elucidated for each polymer structure to achieve balanced properties including water absorbability, ion conductivity, chemical and mechanical stabilities.

We have developed a novel series of partially fluorinated AEMs (QPAF-C1 and QPAF-C1B, Fig. 1) which exhibited reasonable chemical stability because of lack of the heteroatom linkages in the polymer main chains.<sup>14,25</sup> In continuation of our effort to further enhance the chemical stability as well as fuel cell performance and durability, the interstitial side chain strategy was applied to the QPAF

<sup>a</sup> Clean Energy Research Center, University of Yamanashi, 4 Takeda, Kofu 400-8510, Japan

<sup>b</sup> Chemistry Department, Faculty of Science, Sohag University, 825 24, Sohag, Egypt.

† Electronic Supplementary Information (ESI) available: See DOI: 10.1039/x0xx00000x

membranes in this study using facile synthetic methodology starting from the dimethylaminated monomers. Structure and properties of the resulting QPAF-Cx, where x represents number of carbon atoms in the interstitial side chain (C2-C6), were evaluated in detail. A selected membrane with optimum side chain length and properties was subjected to fuel cell operation. The results were compared with those of our benzyl ammonium type QPAF-C1 membranes and a benchmark Tokuyama A201 membrane.

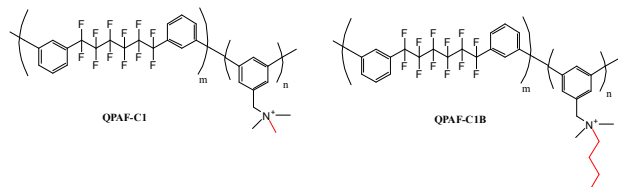


**Fig. 1** Chemical structure of QPAF-C1 and QPAF-C1B.

## 2. Results and discussion

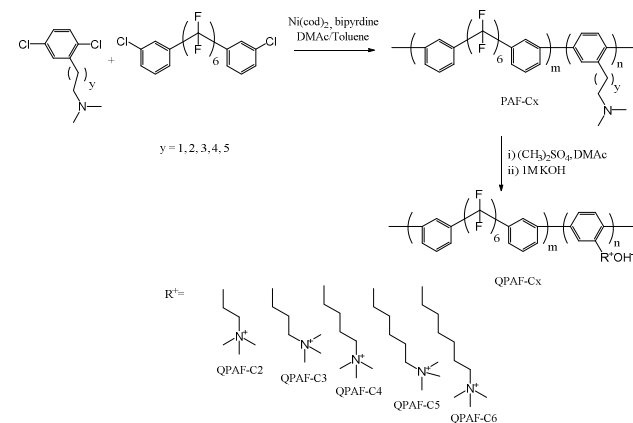
### 2.1. Synthesis of pendant dimethylaminated dichloromonomers

A series of pendant dimethylaminated dichloromonomers containing ethyl, propyl, butyl, pentyl, and hexyl side chains were successfully synthesized from the corresponding carboxylic acid precursors (see Schemes S1-S6 in ESI<sup>†</sup>). Briefly, the carboxylic acid precursors were dimethylamidated via acid chlorination and then reduced with LAH to obtain pure monomers in reasonable total yields (73-89%). The chemical structures of the dimethylaminated dichloromonomers as well as their intermediate compounds were well-characterized by NMR spectra (Figs. S1-S6 in ESI<sup>†</sup>), in which all the aliphatic methylene protons of alkyl side chains were detected at 1.00-2.80 ppm and methyl protons of dimethylamino groups were detected as two singlet peaks at 2.90-3.30 ppm. The aromatic protons were observed at 7.00-7.60 ppm and assigned to the structures. The integral ratios of the peaks further confirm the formation of the pendant dimethylaminated dichloromonomers of the supposed chemical structures.

### 2.2. Synthesis of PAF-Cx copolymers.

The pendant dimethylaminated dichloromonomers were copolymerized with the perfluoromonomer *via* Nickel(0) promoted coupling reaction followed by quaternization reaction with dimethyl sulfate to obtain a series of partially fluorinated copolymers denoted as QPAF-Cx, where x represents number of carbon atoms in the side chains (Scheme 1). The intermediate copolymers (PAF-Cx) were characterized by <sup>1</sup>H and <sup>19</sup>F NMR spectra (Figs. S7-11 in ESI<sup>†</sup>). In the <sup>1</sup>H NMR spectra, benzylic methylene protons appeared at 2.65-2.90 ppm. The methyl protons of dimethylamino groups and interstitial methylene protons were detected at 2.00-2.30 ppm and at 1.00-2.00 ppm, respectively. The <sup>19</sup>F NMR spectra of

PAF-Cx were similar to that of the perfluoromonomer suggesting the absence of any side reactions. The copolymer compositions determined from the integral ratios of the peaks in the <sup>1</sup>H NMR spectra were in fair agreement with the feed comonomer ratios as shown in Table 1. PAF-Cx copolymers had high molecular weights ( $M_w = 37.7-213.4$  kDa,  $M_n = 5.5-19.7$  kDa, polydispersity (PDI) = 3.1-10.7) as determined by GPC analyses. PAF-C2 exhibited the highest molecular weight while its GPC curve contained minor shoulder at lower molecular weight (Fig. S12 in ESI<sup>†</sup>) possibly due to less controlled polymerization reaction.



**Scheme 1** Synthesis of QPAF-Cx copolymers with different side chain lengths.

The PAF-Cx copolymers were quaternized *via* facile and mild procedure using 5 equivolar of dimethyl sulfate as methylating agent to dimethylamino groups and DMAC as solvent to obtain the QPAF-Cx copolymers in methyl sulfate ion forms in high yields (ca. 100%). The quaternized copolymers were characterized by NMR spectra (Figs. S7-11 in ESI<sup>†</sup>). In the <sup>1</sup>H NMR spectra, methyl protons of dimethylamino groups appeared at lower magnetic field (2.70-2.95 ppm) than those of the precursors PAF-Cx (2.00-2.30 ppm) supporting the quaternization reaction. The methylene protons adjacent to dimethylamino groups also shifted to lower magnetic field (3.00-3.20 ppm) from 1.00-2.00 ppm in PAF-Cx. The integral ratios of those peaks confirm complete quaternization reaction. The ion exchange capacity (IEC) of QPAF-Cx was controllable by varying the copolymer compositions. Three different compositions were prepared for each copolymer and the theoretical IEC values ranged from 1.19-1.75 meq. g<sup>-1</sup> (Table 1). The high limit of the IEC value was based on our previous work, in which QPAF-C1 membranes swelled excessively at higher IECs than 1.70 meq. g<sup>-1</sup>.

QPAF-Cx were soluble in some polar organic solvents such as ethanol, NMP, DMSO and DMAC. The pendant aliphatic chains improved the solubility of the QPAF-Cx copolymers in particular in low boiling-point solvents. The copolymers in methyl sulfate ion forms were cast from NMP solution at 60 °C to obtain pale yellow to pale brown transparent membranes. All QPAF-Cx copolymers had good membrane forming

**Table 1** Properties of QPAF-Cx membranes

Membrane	m:n <sup>a</sup>	m:n <sup>b</sup>	$M_w$ (kDa) <sup>c</sup>	$M_n$ (kDa) <sup>c</sup>	PDI <sup>c</sup>	IEC <sub>theo</sub> (meq. g <sup>-1</sup> ) <sup>a</sup>	IEC <sub>NMR</sub> (meq. g <sup>-1</sup> ) <sup>b</sup>	IEC <sub>tit</sub> (meq. g <sup>-1</sup> ) <sup>d</sup>
QPAF-C2	1.0:0.6	1.0:0.6	151.1	17.5	8.6	1.19	1.05	0.98
	1.0:0.9	1.0:0.9	213.4	19.7	10.7	1.50	1.54	1.14
	1.0:1.1	1.0:1.0	114.2	15.8	7.1	1.75	1.56	1.40
QPAF-C3	1.0:0.6	1.0:0.5	84.7	16.0	5.2	1.19	1.04	0.98
	1.0:0.9	1.0:0.9	65.0	9.0	7.1	1.50	1.51	1.24
	1.0:1.2	1.0:1.1	73.2	11.7	6.2	1.75	1.60	1.40
QPAF-C4	1.0:0.7	1.0:0.8	37.7	11.0	3.4	1.19	1.30	1.10
	1.0:0.9	1.0:1.0	40.2	12.0	3.3	1.50	1.51	1.23
	1.0:1.2	1.0:1.1	45.3	14.2	3.1	1.75	1.58	1.50
QPAF-C5	1.0:0.7	1.0:0.7	46.9	7.1	6.5	1.19	1.16	1.02
	1.0:1.0	1.0:1.0	51.6	18.7	3.4	1.50	1.51	1.45
	1.0:1.3	1.0:1.2	55.4	15.4	3.5	1.75	1.72	1.62
QPAF-C6	1.0:0.7	1.0:0.7	61.8	8.3	7.4	1.19	1.14	0.92
	1.0:1.0	1.0:1.0	46.7	5.5	8.5	1.50	1.52	1.40
	1.0:1.3	1.0:1.3	62.2	7.5	8.2	1.75	1.68	1.65

<sup>a</sup> Feed comonomer ratio. <sup>b</sup> Determined by <sup>1</sup>H NMR spectra. <sup>c</sup> Determined by GPC analyses (calibrated with polystyrene standards) for samples before the quaternization. <sup>d</sup> Determined by Mohr titration method (average of three measurements).

capability and provided bendable membranes regardless of their compositions and IEC values. Compared to our previous QPAF-C1 copolymers,<sup>27</sup> the newly prepared QPAF-Cx with aliphatic side chains gave somewhat more flexible membranes presumably because of the more developed interpolymer entanglement *via* longer side chains. The IEC values of the resulting QPAF-Cx membranes were determined from the NMR spectra and by Mohr titration method. The IEC<sub>NMR</sub> values were in fair agreement with the theoretical IEC<sub>theo</sub> values (calculated from the copolymer compositions assuming complete quaternization reaction) while the titrated IEC<sub>tit</sub> values were slightly lower in some cases (Table 1). It is likely that some of the ammonium groups in the membranes did not take part in the ion exchange reaction.

### 2.3. Morphology

The morphology of QPAF-Cx membranes was investigated through TEM images for the membrane samples stained with tetrachloroplatinate ions (Fig. 2). All QPAF-Cx membranes exhibited well-developed phase separated morphology based on the hydrophilic (dark domains) and the hydrophobic (bright domains) differences of the components. It seemed that the phase separation was larger and more distinct as increasing the side chain length. The hydrophilic clusters were ca. 1-4 nm in diameter for QPAF-C2, which were slightly larger in size than those observed for our previous QPAF-C1 membrane (1-2 nm) with comparable IEC.<sup>27</sup> The cluster sizes were 2.4-13.9 nm (QPAF-C3), 2.4-10.5 nm (QPAF-C4), 1.8-12.0 nm (QPAF-C5), and 1.3-14.6 nm (QPAF-C6), respectively. In QPAF-C6 membrane, the ionic clusters aggregated to form even larger ionic domains. The results suggest that the interstitial aliphatic groups separated the pendant ammonium groups from the polymer main chains, resulting in more developed phase-separated morphology. The effect was likely to be more pronounced with longer side chains.

The morphology of QPAF-Cx membranes in chloride ion forms was then elucidated by small angle X-ray scattering

(SAXS) at 40 °C and different humidity. Fig. 3 shows the scattered intensity as a function of the scattering vector ( $q$ ), in which the peak intensities increased as increasing relative humidity (RH), indicating that the peaks were associated with the hydrophilic clusters (ionomer peaks). As increasing the side chain length, the ionomer peak became more prominent and the  $d$  spacing value became larger;  $d$  values corresponded to the mean distances between the periodic structures. The  $d$  value at 90% RH is then plotted as a function of the carbon number in the side chain in Fig. 4. There was a roughly linear relationship between them up to C4. In the background subtracted SAXS profiles (Fig. S13 in ESI<sup>†</sup>), all QPAF-Cx membranes exhibited the same slopes (c.a. -4) in the large  $q$  areas, suggesting the spherical domains of the periodic structure according to Porod's Law.<sup>26</sup> The results are in fair agreement with the above mentioned TEM images, although quantitative comparison between SAXS and TEM data should not be made because of the different counter ions and measurement conditions. The comparison between QPAF-C4 with interstitial butylene groups and QPAF-C1B<sup>14</sup> with pendant butyl groups indicated that the ammonium groups located at the terminal of the side chains promoted more hydrophilic/hydrophobic phase separation.

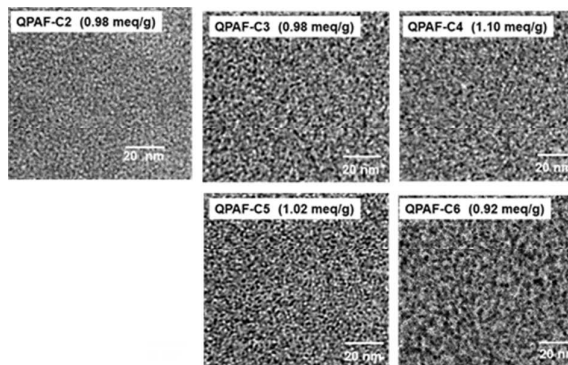


**Fig. 2** TEM images of QPAF-Cx membranes stained with tetrachloroplatinate ions.

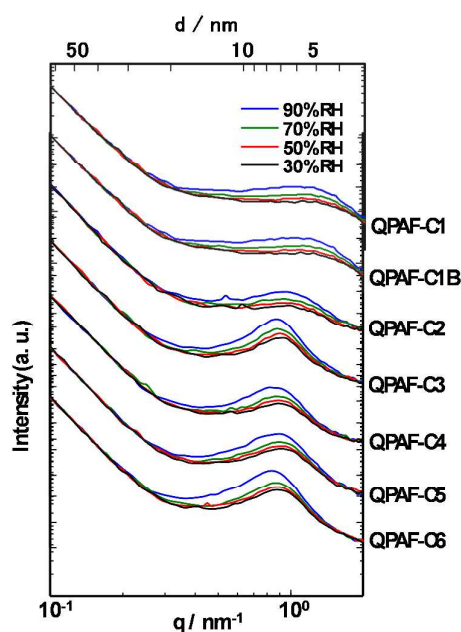


**Fig. 3** SAXS profiles for QPAF-Cx (IEC = 0.92–1.10 meq. g<sup>-1</sup>), QPAF-C1 (IEC = 1.26 meq. g<sup>-1</sup>) and QPAF-C1B (IEC = 1.33 meq. g<sup>-1</sup>) as a function of scattering vector ( $q$ ) between 30% and 90% RH at 40 °C.

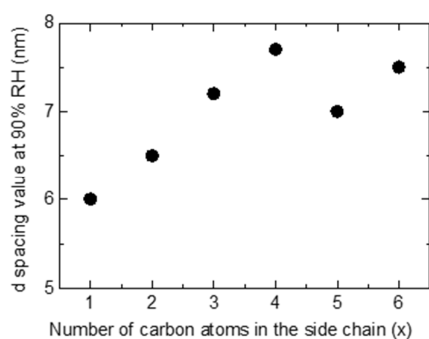


**Fig. 4** Effect of number of carbon atoms in the side chain ( $x$ ) on the  $d$  spacing values of QPAF-Cx membranes at 90% RH (data taken from Fig. 3).

#### 2.4. Water uptake and hydroxide ion conductivity

Since water absorption and management in AEMs are crucial for practical fuel cell applications, water uptake of the QPAF-Cx membranes was measured. Fig. 5 shows the temperature dependence of water uptake of QPAF-Cx membranes with comparable IEC values (0.92–1.26 meq. g<sup>-1</sup>). The general trend was that the water uptake increased as increasing the temperature. In addition, the differences in water uptake among the membranes became larger as increasing the temperature, which caused significant differences in the swelling behaviour at high temperature. In fact, QPAF-C4, -C5, and -C6 membranes became gels above 60 °C and thus, their

water uptakes were not available. QPAF-C1, -C2, and -C3 membranes exhibited smaller water uptake and swelling even at 80 °C. In particular, QPAF-C2 membrane exhibited very low water uptake at wide range of temperature. Comparison between QPAF-C1B and -C4 implied that the membranes absorbed more water when the ammonium groups were attached at the terminal of the aliphatic side chains. At 30 °C, all the membranes did not swell much because of their small water uptake. For example, the swelling ratios of QPAF-C3 membrane with IEC = 0.98 meq. g<sup>-1</sup> were 8% (in-plane) and 14% (through-plane), respectively.

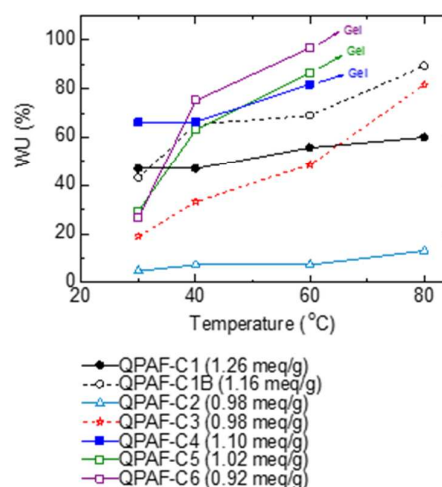


**Fig. 5** Temperature dependence of water uptake (WU) of QPAF-Cx and QPAF-C1B membranes.

Another important property of AEMs is ion conductivity, which is related with IEC and water affinity. In the present study, in-plane hydroxide ion conductivity was measured. Since AEMs tend to absorb carbon dioxide quickly from the ambient air,<sup>29,30</sup> contact with air was avoided for QPAF-Cx membranes in hydroxide ion forms before the measurement to obtain pure hydroxide ion conductivity. The hydroxide ion conductivity of QPAF-Cx membranes at 30 °C is plotted as a function of IEC in Fig. 6. QPAF-C3, -C4, -C5, and -C6 membranes exhibited similar behavior to QPAF-C1;<sup>27</sup> the conductivity increased as increasing IEC then showed a plateau or slight decrease at higher IEC than 1.50 meq. g<sup>-1</sup> due to the high swelling with water causing loss in substantial IEC. QPAF-C2 exhibited the smallest hydroxide ion conductivity related with its smallest water uptake. Compared to QPAF-C4, QPAF-C1B membrane exhibited ion conductivity much more dependent on IEC because the latter showed small swelling even for high IEC membranes to maintain the substantial IEC high.

For the quantitative discussion on the effect of the side chain length, the water uptake and hydroxide ion conductivity at 60 °C are re-plotted as a function of  $x$  (carbon atoms in spacer unit) in Fig. 7. The water uptake dropped significantly from C1 to C2, and then increased from C2 to C6. The results (in particular for C1 and C2) were not correlated with the effect of the side chain length on the morphology, in which hydrophilic domains developed more as increasing the carbon number in the side chain. The ion conductivity exhibited

similar  $x$  dependence to that of water uptake because the ion conduction was mainly dominated by the absorbed water molecules in the hydrophilic domains. However, excess water (e.g., > 20 water molecules per ammonium group for -C4, -C5 and -C6 membranes) in the hydrophilic domains diluted the ionic concentration to cause a decrease in ion conductivity.

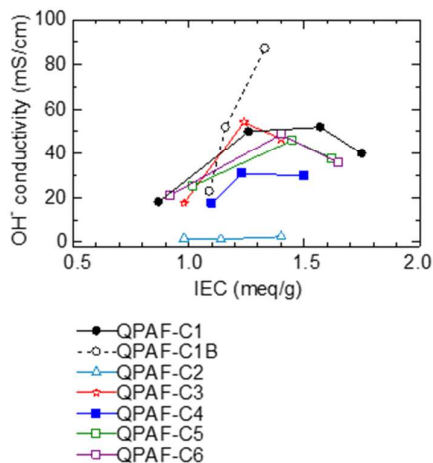


**Fig. 6** Hydroxide ion conductivity of QPAF-Cx and QPAF-C1B membranes at 30 °C in water as a function of IEC.

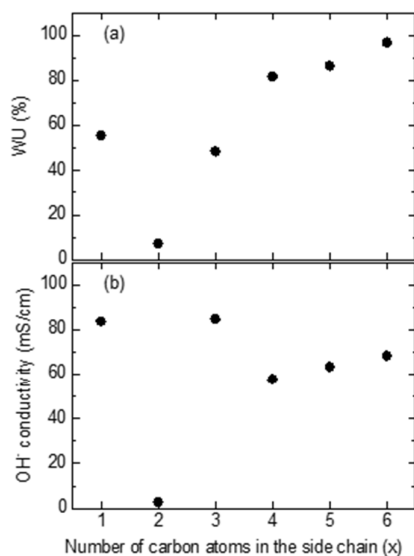


**Fig. 7** Effect of number of carbon atoms in the side chain ( $x$ ) on (a) water uptake (WU) and (b) hydroxide ion conductivity of QPAF-Cx membranes at 60 °C in water.

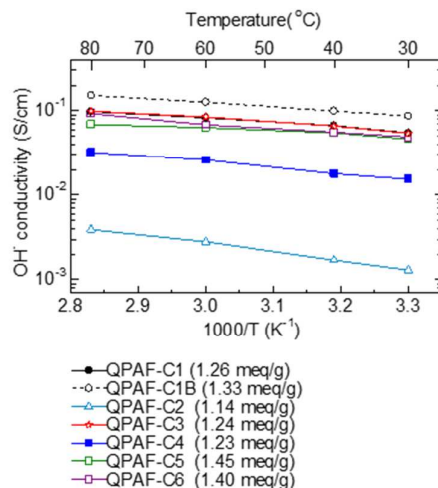


**Fig. 8** Temperature dependence of the hydroxide ion conductivity of QPAF-Cx and QPAF-C1B membranes in water.

Temperature dependence of the hydroxide ion conductivity of QPAF-Cx membranes is shown in Fig. 8. All QPAF-Cx membranes showed approximate Arrhenius-type temperature dependence of the conductivity. Among them, QPAF-C3 (1.24 meq. g<sup>-1</sup>) achieved the highest conductivity (99 mS cm<sup>-1</sup>) at 80 °C followed by QPAF-C1 (1.26 meq. g<sup>-1</sup>, 98 mS cm<sup>-1</sup>), QPAF-C6 (1.40 meq. g<sup>-1</sup>, 93 mS cm<sup>-1</sup>), QPAF-C5 (1.45 meq. g<sup>-1</sup>, 69 mS cm<sup>-1</sup>), QPAF-C4 (1.23 meq. g<sup>-1</sup>, 64 mS cm<sup>-1</sup>), and QPAF-C2 (1.5 meq. g<sup>-1</sup>, 4 mS cm<sup>-1</sup>), respectively. QPAF-C1B (1.33 meq. g<sup>-1</sup>) exhibited even higher conductivity (152 mS cm<sup>-1</sup>) because of its low swelling under the same conditions.<sup>14,27</sup> The apparent activation energies ( $E_a$ ) calculated from the slopes were, 9.9 kJ mol<sup>-1</sup> (QPAF-C1), 10.0 kJ mol<sup>-1</sup> (QPAF-C1B), 10.5 kJ mol<sup>-1</sup> (QPAF-C3), 6.5 kJ mol<sup>-1</sup> (QPAF-C4), 6.8 kJ mol<sup>-1</sup> (QPAF-C5), 11.0 kJ mol<sup>-1</sup> (QPAF-C6), respectively, and were comparable to those of our previous AEMs, suggesting conduction mechanism involving hydrated ions.<sup>14,27</sup> QPAF-C2 membrane exhibited higher  $E_a$  (19.6 kJ mol<sup>-1</sup>) than those of the other membranes due to the small water uptake and thus undeveloped ionic channels even under the wet conditions.

## 2.5. Alkaline stability

The alkaline stability of QPAF-Cx membranes was first tested in 1 M KOH at 80 °C (Fig. S14 in ESI<sup>†</sup>). Note that the initial increase in the conductivity was due to ion exchange to hydroxide ions. QPAF-C3 (0.98 meq. g<sup>-1</sup>) and QPAF-C4 (1.10 meq. g<sup>-1</sup>) showed good alkaline stability with high remaining conductivity (24 mS cm<sup>-1</sup>, 82% and 24 mS cm<sup>-1</sup>, 73%, respectively) after 1000 h. These membranes were more stable than benzylammonium-type QPAF-C1 (1.26 meq. g<sup>-1</sup>) and QPAF-C1B (1.00 meq. g<sup>-1</sup>) whose remaining conductivities were 1 mS cm<sup>-1</sup> (5%) after 500 h and 14 mS cm<sup>-1</sup> (68%) after 700 h, respectively.<sup>14,27</sup> The results suggest that the interstitial aliphatic groups (C3 and C4) mitigated the degradation of the ammonium groups from the nucleophilic attack of the hydroxide ions, and are in fair agreement with those reported in the literature.<sup>21–26</sup> QPAF-C2 also exhibited high stability (80%

of the remaining after 700 h), although its initial conductivity was much lower than the other membranes as discussed above. QPAF-C5 and QPAF-C6 membranes swelled very much in the alkaline solution and the stability test was unavailable.

The results motivated us to investigate the alkaline stability of QPAF-C3 and QPAF-C4 membranes under severer conditions such as 4 M and 8 M KOH at 80 °C (Fig. 9). Both membranes survived in 4 M KOH for 1000 h with high remaining conductivity (24 mS cm<sup>-1</sup>, 74% and 26 mS cm<sup>-1</sup>, 80%, respectively). However, the conductivity dropped in 8 M KOH after 568 h to 4 mS cm<sup>-1</sup> (8% remaining) for QPAF-C3 and 8 mS cm<sup>-1</sup> (25% remaining) for QPAF-C4, respectively, indicating considerable degradation of the ammonium groups.

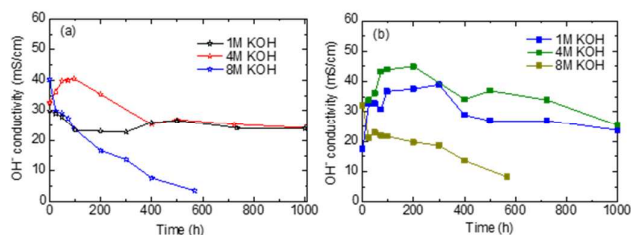


**Fig. 9** Time course of hydroxide ion conductivity (at 40 °C) of (a) QPAF-C3 (0.98 meq. g<sup>-1</sup>) and (b) QPAF-C4 (1.10 meq. g<sup>-1</sup>) membranes in 1 M, 4 M and 8 M KOH at 80 °C.

To investigate the effect of IEC value on the alkaline stability, higher IEC membrane was also tested (Fig. S15 in ESI<sup>†</sup>). QPAF-C3 (1.24 meq. g<sup>-1</sup>) exhibited excellent stability with high remaining conductivity (59 mS cm<sup>-1</sup>, 98% in 1 M KOH and 43 mS cm<sup>-1</sup>, 73% in 4 M KOH) after 1000 h. However, the conductivity decreased to 8 mS cm<sup>-1</sup> (14% remaining) in 8 M KOH after 568 h. The results are similar to those of the lower IEC QPAF-C3 (0.98 meq. g<sup>-1</sup>) and suggest that the alkaline degradation was not much dependent on IEC but the chemical structure of the ammonium groups.

Unlike our previous QPAF-C1 and QPAF-C1B membranes which became insoluble after the alkaline stability tests,<sup>14,27</sup> the QPAF-Cx membranes with pendant ammonium groups retained solubility in organic solvents which enabled us post-test NMR analyses. As shown in Fig. 10a, <sup>1</sup>H NMR spectra of QPAF-C3 (0.98 meq. g<sup>-1</sup>) showed undetectable changes even after 1000 h in 1 M and 4 M KOH at 80 °C. The higher magnetic field shift of the peak (8) of the sample after 1000 h in 4 M KOH was attributed to some stereo-conformational changes rather than degradation as suggested by 2D COSEY NMR spectra (Fig. S16 in ESI<sup>†</sup>) since the shifted peak was interacted with the adjacent protons (peaks 7, 9). However, the zoomed-in NMR spectra of the sample after 568 h in 8 M KOH revealed a small peak at ca. 6.5 ppm indicative of minor Hofmann degradation. There observed no practical changes in the <sup>19</sup>F NMR spectra (Fig. 10b) for the three post-test samples, indicating that the perfluoroalkylene moieties in the main chain were intact during the harsh alkaline stability tests. In the NMR spectra of the post-test higher IEC QPAF-C4 (1.10 meq. g<sup>-1</sup>) in 4 M and 8 M KOH (Fig. S17 in ESI<sup>†</sup>), small and broad peaks were detected at ca. 2.0 ppm and at 4.8–6.0 ppm

(in the zoomed-in spectra) ascribed to nucleophilic substitution and Hofmann elimination, respectively.

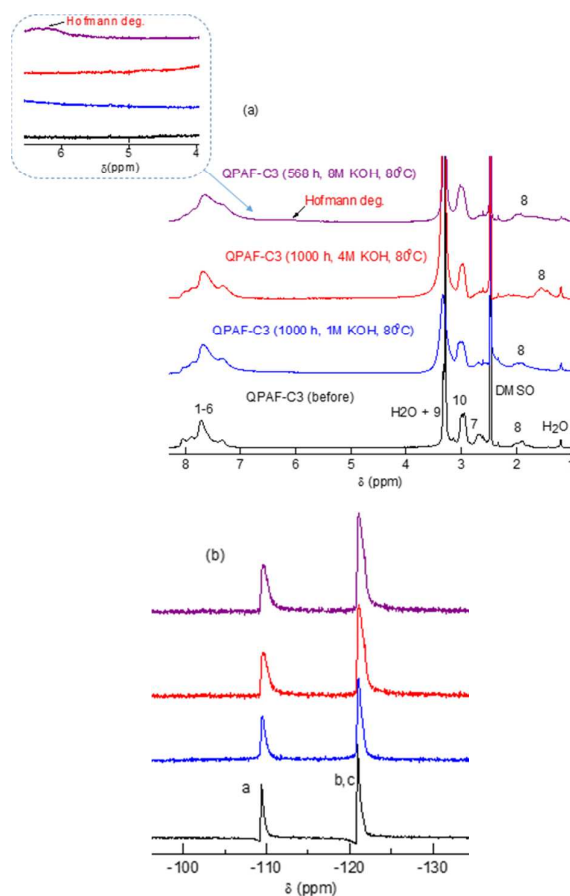


**Fig. 10** (a) <sup>1</sup>H and (b) <sup>19</sup>F NMR spectra of QPAF-C3 membranes (0.98 meq. g<sup>-1</sup>) in DMSO-*d*<sub>6</sub> after the alkaline stability test.

In Table 2, the IEC values determined from titration and <sup>1</sup>H NMR spectra of the pristine and the post-test QPAF-C3 and -C4 membranes are summarized. The losses in IEC values were minor even after the testing in 8 M KOH. For example, the post-test QPAF-C3 (1.24 meq. g<sup>-1</sup>) membrane after 568h in 8 M KOH retained 71% of IEC<sub>tit</sub> and 92% of IEC<sub>NMR</sub>, however, the remaining conductivity was 9 mS cm<sup>-1</sup> (14%). QPAF-C4 (1.10 meq. g<sup>-1</sup>) membrane retained 76% of IEC<sub>NMR</sub> under the same conditions, however, the remaining conductivity was 8 mS cm<sup>-1</sup> (26%). The results suggest that, even when the chemical degradation of the ammonium groups was minor, the anion conduction could be hampered by other factors.

**Table 2** IEC values of the post-test QPAF-C3 and -C4 membranes

Membrane	Alkaline conditions (M KOH)	IEC <sub>tit</sub> before (meq. g <sup>-1</sup> )	IEC <sub>tit</sub> After (meq. g <sup>-1</sup> )	Remaining IEC <sub>tit</sub> (%)	IEC <sub>NMR</sub> After (meq. g <sup>-1</sup> )	Remaining IEC <sub>NMR</sub> (%)	Conductivity After (mS cm <sup>-1</sup> )	Remaining Conductivity (%)
QPAF-C3	1	0.98	0.88	90	0.76	73	24	80
	4	0.98	0.83	85	1.00	96	24	74
	8	0.98	N/A <sup>a</sup>	N/A <sup>a</sup>	0.97	93	4	9
	4	1.24	0.95	77	1.45	96	43	73
	8	1.24	0.88	71	1.38	92	9	14
QPAF-C4	1	1.10	0.95	86	1.18	91	24	73
	4	1.10	0.96	87	1.12	86	26	80
	8	1.10	N/A <sup>a</sup>	N/A <sup>a</sup>	0.99	76	8	26

<sup>a</sup> Samples not enough for titration.

To clarify the reason behind such conductivity drop, the post-test morphology study of QPAF-C3 (0.98 meq. g<sup>-1</sup>) and -C4 (meq. g<sup>-1</sup>) membranes was carried out through TEM images (Fig. S18 in ESI<sup>†</sup>). In general, all of the post-test membranes retained their phase-separated morphology. However, in the post-test membranes, hydrophilic domains became significantly smaller than those of the pristine membranes from 2.4-13.9 nm (pristine) to 0.5-5.2 nm (post-test) for QPAF-C3 and from 2.4-10.5 nm (pristine) to 0.5-4.5 nm (post-test) for QPAF-C4 membranes, respectively. In addition, the ionic clusters were inhomogeneously distributed causing less ordered ionic channels with insufficient interconnectivity, in particular, for higher IEC (1.10 meq. g<sup>-1</sup>) QPAF-C4 membrane. Such morphological changes could have been brought about during the harsh alkaline stability tests causing significant drop in the ion conductivity.

## 2.6. Mechanical properties

The mechanical properties of QPAF-Cx membranes were investigated through DMA analyses at 60% RH from 25-95 °C (Fig. 11). Samples in chloride ion forms were used to avoid the effect of carbon dioxide from the environment. The initial values of storage modulus ( $E'$ ), loss modulus ( $E''$ ) and  $\tan \delta$  ( $= E''/E'$ ) at 25 °C were similar but the temperature dependence differed among the membranes. QPAF-C1 exhibited slight loss in  $E'$  above ca. 70 °C and a broad peak in  $E''$  at ca. 85 °C. The loss in  $E'$  and the peak in  $E''$  appeared at lower temperature for QPAF-C1B and even lower for QPAF-Cx as increasing the side chain length. To investigate quantitatively the effect of the side chain length on the viscoelastic properties, the peak temperature in  $\tan \delta$  is plotted as a function of x in Fig. S19 (in ESI<sup>†</sup>), in which the transition temperature lowered as increasing the side chain length with seemingly odd/even effect. The results suggest that the transition temperatures observed as the peaks in  $\tan \delta$  curves were associated with the side chain motion.

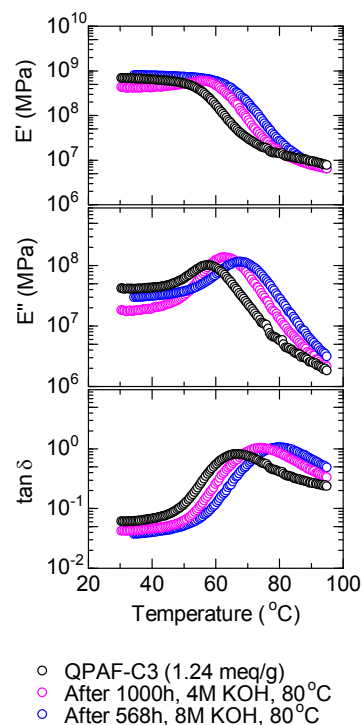


**Fig. 11** DMA curves of QPAF-Cx membranes as a function of temperature at 60% RH.

After the alkaline stability test, DMA analysis was performed for QPAF-C3 as the most durable membrane among QPAF-Cx series (Fig. 12). In both cases, after 1000 h in 4 M KOH and after 568 h in 8 M KOH, the loss in  $E'$  and the peaks in  $E''$  and  $\tan \delta$  appeared at higher temperatures than those of the pristine QPAF-C3 membrane. The changes in the DMA properties are possibly associated with the minor Hofmann degradation in the side chains and morphological changes during the stability tests.

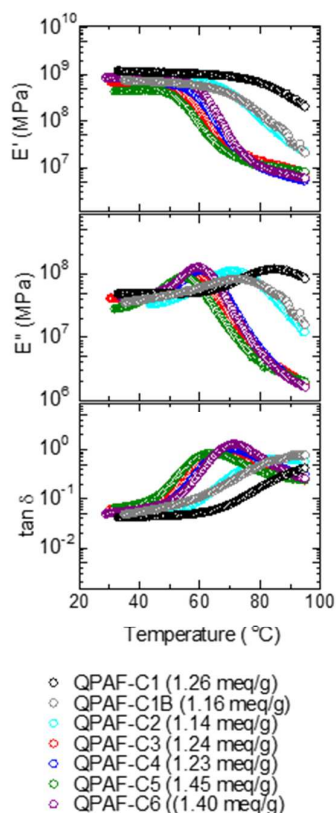


**Fig. 12** DMA curves of QPAF-C3 membrane as a function of temperature at 60% RH before and after the alkaline stability test.

The elongation properties of QPAF-C3 and -C4 membranes were then investigated through stress-strain curves at 60 °C and 60% RH as shown in Fig. 13. QPAF-C3 (1.24 meq. g<sup>-1</sup>) exhibited higher elongation at break (135%) and yield stress (9.5 MPa) than those of QPAF-C4 (1.23 meq. g<sup>-1</sup>) (89% and 8.7 MPa, respectively). The lower IEC QPAF-C3 (0.98 meq. g<sup>-1</sup>) membrane exhibited even higher elongation at break (173%) and yield stress (17.2 MPa). Compared to our previous QPAF-C1B (1.16 meq. g<sup>-1</sup>) membrane that exhibited 55% of the elongation and 14.6 MPa of the yield stress, QPAF-C3 membranes exhibited much higher strain at break, which make them more promising for practical fuel cell applications. For more quantitative analysis of the effect of side chain length on the elongation properties, the elongation at break and maximum stress of QPAF-Cx membranes are plotted as a function of x (Fig. S20 in ESI<sup>†</sup>). Similar to the viscoelastic properties, the maximum stress decreased as increasing the side chain in particular when the side chain became longer than two carbons. The elongation at break showed a distinct even/odd effect with high elongation for odd carbon-numbered side chains. From these results, we confirm that QPAF-C3 membrane exhibited the most balanced properties with high hydroxide ion conductivity, good alkaline stability and reasonable mechanical properties among the QPAF-Cx membranes.

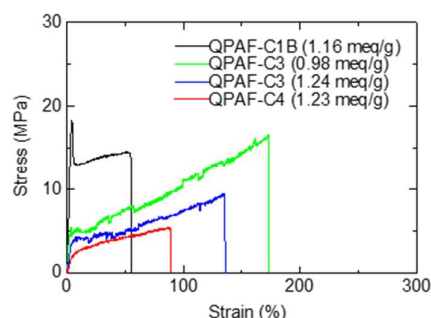


**Fig. 13** Stress-strain curves of QPAF-C3, -C4, and QPAF-DMBA membranes at 60 °C and 60% RH.

## 2.7. Fuel cell performance

A catalyst coated membrane (CCM) was prepared with QPAF-C3 membrane (IEC = 1.24 meq. g<sup>-1</sup>, 50 μm thick) as membrane and QPAF-C3 (IEC = 0.98 meq. g<sup>-1</sup>) as electrode binder, using Pt/C for both anode and cathode catalysts. For reference, another CCM with Tokuyama A201 (IEC = 1.7 meq. g<sup>-1</sup>, 28 μm thick) as membrane and AS-4 (IEC = 1.4 meq. g<sup>-1</sup>) as electrode binder was also prepared. Fuel cells were operated under the same conditions at 60 °C and 100% RH for both O<sub>2</sub> and H<sub>2</sub>. As shown in Fig. 14, both cells exhibited high open circuit voltage (OCV), 1.01 V for QPAF-C3 and 1.03 V for Tokuyama A201, respectively, suggesting low gas permeability of QPAF-C3 membrane similar to our previous QPAF-C1 (1.01 V) and QPAF-C1B (1.03 V) membranes.<sup>14,27</sup> The ohmic resistance of the QPAF-C3 cell was ca. 0.22 Ω cm<sup>2</sup>, which was higher than that (0.059 Ω cm<sup>2</sup>) calculated from the hydroxide ion conductivity of QPAF-C3 membrane in water (85 mS cm<sup>-1</sup> at 60 °C, Fig. 7) presumably due to the contact resistance with the catalyst layers and lower ion conductivity at 100% RH than in water. Despite its thicker thickness, QPAF-C3 membrane exhibited comparable ohmic resistance to that of Tokuyama A201 (0.20 Ω cm<sup>2</sup>) indicating higher ion conductivity of QPAF-C3 membrane. QPAF-C3 cell was operable to higher current density than that of Tokuyama A201 cell. The maximum power density of QPAF-C3 cell was 224 mW cm<sup>-2</sup>, ca. 1.8 times higher than that of Tokuyama A201 cell (122 mW cm<sup>-2</sup>) and even higher than those of our previous QPAF-C1B (167 mW cm<sup>-2</sup>) and QPAF-C1 (138 mW cm<sup>-2</sup>) cells. Taking low Pt-loading (0.2 mg cm<sup>-2</sup>) into account, the power density per platinum mass was as high as 1120 mW mgPt<sup>-1</sup>.

As a durability test, the fuel cells were operated at a constant current density (50 mA cm<sup>-2</sup>) and the cell potentials were monitored (Fig. 15). The ohmic resistance increased slightly for both cells, from 0.22 to 0.50 Ω cm<sup>2</sup> for QPAF-C3 and from 0.22 to 0.42 for Tokuyama A201, respectively after 62 h. The increases in ohmic resistance implied some degradation of the membranes. The degradation was more serious in the cell voltages. After 62 h operation, the cell voltages were 0.57 V (69% remaining) for QPAF-C3 cell and 0.42 V (52% remaining) for Tokuyama A201 cell, respectively. After the durability test, QPAF-C3 membrane was recovered by carefully removing the catalyst layers. The <sup>1</sup>H and <sup>19</sup>F NMR spectra of the post durability test membrane did not show evidences of the structural changes (Fig. S21 in ESI<sup>†</sup>). The results suggest that QPAF-C3 was substantially stable as membrane in operating

fuel cell, while may degrade (or experience morphological changes similar to the ex-situ alkaline stability test discussed above) as electrode binder. As Dekel and his co-workers recently reported,<sup>10,31,32</sup> hydration number of the hydroxide ions could become much lower in operating fuel cells than in concentrated KOH aqueous solution, ammonium groups were likely to degrade faster in the fuel cell. The longevity of the fuel cell in this study was among the best reported so far.<sup>33</sup>

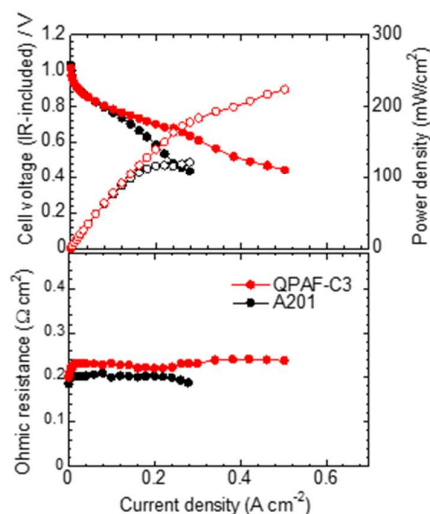


**Fig. 14**  $\text{H}_2/\text{O}_2$  fuel cell performance for QPAF-C3 ( $1.24 \text{ meq. g}^{-1}$ ) as membrane and QPAF-C3 ( $0.98 \text{ meq. g}^{-1}$ ) as electrode binder in comparison with Tokuyama A201 ( $1.7 \text{ meq. g}^{-1}$ ) as membrane and AS-4 ( $1.4 \text{ meq. g}^{-1}$ ) as electrode binder at  $60^\circ\text{C}$  and 100% RH.

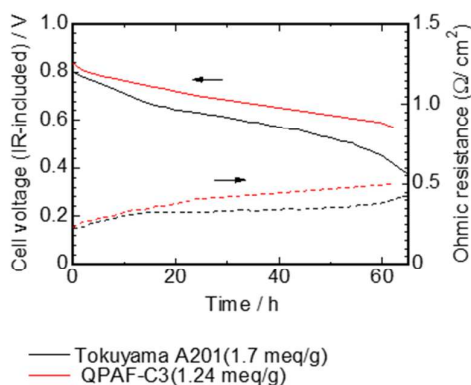


**Fig. 15** Changes of cell potential and ohmic resistance of fuel cells. The cells were operated at  $60^\circ\text{C}$  and 100% RH at a constant current density ( $50 \text{ mA cm}^{-2}$ ).

### 3. Conclusions

The effect of aliphatic side chain length on the properties of QPAF membranes was investigated in detail. The interstitial

aliphatic groups between the polymer main chains and the ammonium groups improved the solubility and flexibility of the resulting QPAF-Cx membranes compared to our previous benzylammonium-type QPAF-C1 and -C1B membranes. Introducing side chains with C3 and longer contributed to well-developed phase-separated morphology as confirmed by TEM images and SAXS measurement. The longer side chains caused higher water affinity and this effect was more pronounced with C4 and longer. The hydroxide ion conductivity exhibited similar dependence on the side chain length to that of water uptake, suggesting that the ion conduction was dominated by the absorbed water molecules in the hydrophilic domains. QPAF-C3 membrane achieved the balanced properties of high ion conductivity with low water uptake. There seemed odd/even effect of the side chain length on mechanical properties, lower thermal transition temperature and higher elongation at break for polymer membranes with odd-numbered carbon side chains. QPAF-C3 and -C4 membranes exhibited alkaline stability for long time under harsh alkaline conditions (1 M and 4 M KOH at  $80^\circ\text{C}$ ), whereas membranes with longer side chains did not survive due to excess swelling. In 8 M KOH, however, QPAF-C3 and -C4 membranes showed a gradual loss in the conductivity. The post-test NMR, titration, and TEM analyses revealed that minor chemical degradation and some morphological changes seemed responsible for the loss in the conductivity. An  $\text{H}_2/\text{O}_2$  fuel cell with QPAF-C3 membrane exhibited high power density of  $224 \text{ mW cm}^{-2}$  that was higher than those with our previous QPAF-C1 and Tokuyama A201 membranes. QPAF-C3 maintained 69% of its initial voltage after 62 h fuel cell durability test that was also superior to Tokuyama A201 (52% remaining voltage). The voltage loss in QPAF-C3 was referred to the electrode binder degradation and/or morphological relaxation but not structural degradation as confirmed by post-test NMR analyses. The results suggest that introducing interstitial aliphatic side chain caused significant improvement not only in the alkaline stability of the membranes but also in the cell performance and durability.

### Conflicts of interest

There are no conflicts to declare.

### Acknowledgements

This work was partly supported by CREST (JPMJCR12C3), Japan Science and Technology Agency (JST) and the Ministry of Education, Culture, Sports, Science and Technology (MEXT) Japan through a Grant-in-Aid for Scientific Research (18H02030). K.M. acknowledges the Ogasawara Foundation for the Promotion of Science and Engineering for financial support. We thank Mr. Taro Kimura for SAXS measurements and Mr. Kanji Otsuji for fuel cell experiments.

### Notes and references

- F. Rahman and M. Skyllas-Kazacos, *J. Power Sources*, 2009, **189**, 1212-1219.
- D. Chen, M. A. Hickner, E. Agar and E. C. Kumbur, *Electrochem. Commun.*, 2013, **26**, 37-40.
- Y. Wang, Z. Zhang, C. Jiang and T. Xu, *Ind. Eng. Chem. Res.* 2013, **52**, 18356-18361.
- M. Carmo, D. L. Fritz, J. Mergel and D. Stolten, *Int. J. Hydrogen Energy*, 2013, **38**, 4901-4934.
- J. R. Varcoe, P. Atanassov, D. R. Dekel, A. M. Herring, M. A. Hickner, P. A. Kohl, A. R. Kucernak, W. E. Mustain, K. Nijmeijer, K. Scott, T. Xu and L. Zhuang, *Energy Environ. Sci.*, 2014, **7**, 3135-3191.
- Y.-J. Wang, J. Qiao, R. Baker and J. Zhang, *Chem. Soc. Rev.*, 2013, **42**, 5768-5787.
- Z. Zhang, E. Chalkova, M. Fedkin, C. Wang, S. N. Lvov, S. Komarneni and T. C. M. Chung, *Macromolecules*, 2008, **41**, 9130-9139.
- H. Long, K. Kim and B. S. Pivovar, *J. Phys. Chem. C*, 2012, **116**, 9419-9426.
- Y.-K. Choe, C. Fujimoto, K.-S. Lee, L. T. Dalton, K. Ayers, N. J. Henson and Y. S. Kim, *Chem. Mater.*, 2014, **26**, 5675-5682.
- D. R. Dekel, M. Amar, S. Willdorf, M. Kosa, S. Dhara and C. E. Diesendruck, *Chem. Mater.*, 2017, **29**, 4425-4431.
- S. Gottesfeld, D. R. Dekel, M. Page, C. Bae, Y. Yan, P. Zelenay and Y. S. Kim, *J. Power Sources*, 2018, **375**, 170-184.
- N. Li, Y. Leng, M. A. Hickner and C. Y. Wang, *J. Am. Chem. Soc.*, 2013, **135**, 10124-10133.
- H.-S. Dang and P. Jannasch, *Macromolecules*, 2015, **48**, 5742-5751.
- A. M. A. Mahmoud, A. M. M. Elsaghier and K. Miyatake, *Macromolecules*, 2017, **50**, 4256-4266.
- J. Pan, J. Han, L. Zhu and M. A. Hickner, *Chem. Mater.*, 2017, **29**, 5321-5330.
- D. S. Kim, A. Labouriau, M. D. Guiver and Y. S. Kim, *Chem. Mater.*, 2011, **23**, 3795-3797.
- Y. Zha, M. L. Disabb-Miller, Z. D. Johnson and M. A. Hickner, *J. Am. Chem. Soc.*, 2012, **134**, 4493-4496.
- A. G. Wright, J. Fan, B. Britton, T. Weissbach, H.-F. Lee, E. A. Kitching, T. J. Peckham and S. Holdcroft, *Energy Environ. Sci.*, 2016, **9**, 2130-2142.
- B. Shi, Y. Li, H. Zhang, W. Wu, R. Ding, J. Dang and J. Wang, *J. Membr. Sci.*, 2016, **498**, 242-253.
- H. Zhang, B. Shi, R. Ding, H. Chen, J. Wang and J. Liu, *Ind. Eng. Chem. Res.*, 2016, **55**, 9064-9076.
- A. D. Mohanty and C. Bae, *J. Mater. Chem. A*, 2014, **2**, 17314-17320.
- W. H. Lee, A. D. Mohanty and C. Bae *ACS Macro Lett.*, 2015, **4**, 453-457.
- M. Zhang, J. Liu, Y. Wang, L. An, M. D. Guiver and N. Li, *J. Mater. Chem. A*, 2015, **3**, 12284-12296.
- S. A. Nuñez, C. Capparelli and M. A. Hickner, *Chem. Mater.* 2016, **28**, 2589-2598.
- H. Ono, T. Kimura, A. Takano, K. Asazawa, J. Miyake, J. Inukai and K. Miyatake, *J. Mater. Chem. A*, 2017, **5**, 24804-24812.
- R. Akiyama, N. Yokota, K. Otsuji and K. Miyatake, *Macromolecules*, 2018, **51**, 3394-3404.
- H. Ono, J. Miyake, S. Shimada, M. Uchida and K. Miyatake, *J. Mater. Chem. A*, 2015, **3**, 21779-21788.
- G. Porod, *Kolloid Z.* 1951, **124**, 83-114.
- N. Ziv, W. E. Mustain and D. R. Dekel, *ChemSusChem*, 2018, **11**, 1136-1150.
- N. Ziv and D. R. Dekel, *Electrochem. Commun.*, 2018, **88**, 109-113.
- D. R. Dekel, S. Willdorf, U. Ash, M. Amar, S. Pusara, S. Dhara, S. Srebnik and C. E. Diesendruck, *J. Power Sources*, 2018, **375**, 351-360.

32 C. E. Diesendruck and D. R. Dekel, *Curr. Opin. Electrochem.*, 10.1016/j.coelec.2018.03.019.

33 D. R. Dekel, *J. Power Sources*, 2018, **375**, 158-169.

## Graphical Abstract

Partially fluorinated aromatic polymer-based anion exchange membranes with propylene side chain exhibit high chemical stability and alkaline fuel cell performance.

